Letter

A Frequency Domain Analysis of the Excitability and Bifurcations of the FitzHugh−Nagumo Neuron Model

Juan Bisquert*

Read Online

ACCESS | Metrics & More | Article Recommendations | Supporting Information

ABSTRACT: The dynamics of neurons consist of oscillating patterns of a membrane potential that underpin the operation of biological intelligence. The FitzHugh−Nagumo (FHN) model for neuron excitability generates rich dynamical regimes with a simpler mathematical structure than the Hodgkin−Huxley model. Because neurons can be understood in terms of electrical and electrochemical methods, here we apply the analysis of the impedance response to obtain the characteristic spectra and their evolution as a function of applied voltage. We convert the two nonlinear differential equations of FHN into an equivalent circuit model, classify the different impedance spectra, and calculate the corresponding trajectories in the phase plane of the variables. In analogy to the field of electrochemical oscillators, impedance spectroscopy detects the Hopf bifurcations and the spiking regimes. We show that a neuron element needs three essential internal components: capacitor, inductor, and negative differential resistance. The method supports the fabrication of memristor-based artificial neural networks.
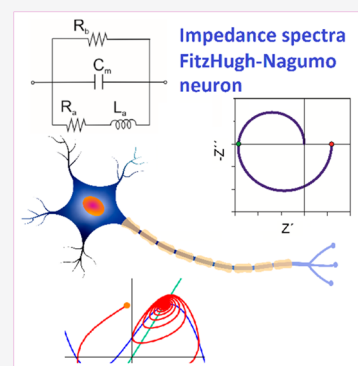
A brain is a complex structure where computing and memory are tightly intertwined, conducted by large networks of neurons connected by synapses. Individual neurons function by gated ion channels that undergo positive and negative membrane voltage feedback cycles in response to multiple incoming stimuli. The neuronal activation triggers voltage spikes of equal magnitude at a variable rate.[1] Understanding the firing patterns of neurons and the coupled oscillations of neuronal ensembles allows us to better understand the operation of the brain. Furthermore, the neuronal firing patters are the key component of neuromorphic engineering, which aims to design and build artificial neural systems, like computational arrays of synapse-connected artificial neurons, retinomorphic vision systems, or auditory processors, using (micro)electrical components and circuits.[2,3] Massively parallel brain-inspired in-memory computing operations may bring much needed advances in the spatial density of computational resources and power consumption and overcome the Von-Neumann bottleneck.[4−7] These model biological systems are adaptive, fault tolerant, and scalable and process information using energy-efficient, asynchronous, event-driven methods, well suited to cognition and motor tasks. It is already possible to create functional elements for the construction of biomimetic computational systems such as spiking neural networks (SNNs) based on memristor elements,[8,9] such as NbO spiking neuristors.[10,11]

The technique of small-amplitude impedance spectroscopy (IS) is widely used in electrochemistry and materials science for the analysis of physicochemical processes and the characterization of experimental parameters.[12] The modulated current in response to a small periodic perturbation of voltage with angular frequency ω is measured. The resulting linear impedance data are described in terms of an equivalent circuit (EC) model that provides detailed information about the physical processes occurring at different time and frequency scales. Investigating the frequency domain response allows one to decompose the response of a device into a set of characteristic spectra that can be readily recognized. The method is used widely in biophysics[13−16] and can be applied to memristors and neuron models.[17]

The impedance measurements were important historically for deriving the paradigm of membrane excitability by Hodgkin and Huxley (HH)[18] that underpins the current understanding of neuronal activity.[19] Early in the 20th century, the membrane was found to have a frequency-dependent impedance.[20,21] The main early neuron models, such as Lapicque's 1907 integrate-and-fire model,[22] the 1952 HH model,[18] and that of Nagumo et al.,[23] analyzed the neuronal activity using the methods of electrical circuits. However, in later years the time domain methods prevailed, and the IS properties of neurons have not been systematically described, to the best of our knowledge. Here we aim to provide tools for the characterization of the dynamical properties of neurons, by analysis of a representative dynamical model in the frequency domain. We want to obtain a
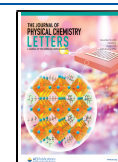
classification of spectra corresponding to different dynamical behaviors of the neuron.

To describe neuronal response and behavior, we adopt dynamical models formed by a nonlinear set of differential equations that emulate the actual output of a biological neuron.[24−26] HH is a complete description of an excitable membrane by the concerted actuation of several ion channels, but it is computationally complex as it involves the membrane voltage and three different internal state variables. Simpler models can generate many dynamical properties of the neurons. A minimal dynamical model is composed of a two-dimensional system that contains the evolution of membrane potential u and a slower "recovery" variable w.[27] The first minimal model was developed in 1961 by FitzHugh[28] by reducing the three slow variables of the HH model to just one refractory current. Nagumo et al.[25] formulated the model in an electrical analogy, including inductor and negative resistance elements. The resulting FitzHugh−Nagumo (FHN) model displays realistic neural dynamics like the cessation of repetitive spiking as the amplitude of the stimulus current increases.[23,27] It has also been broadly studied by its rich phase portraits, as described in books and review articles,[27,29−31] and it is computationally efficient for analyzing the dynamics of neural networks.[32,33] The dynamics of systems of coupled FHN neurons and their bifurcation properties have been amply studied in recent years.[34−39]

There are several motivations for studying the impedance spectroscopy of neurons.

(1) The impedance of neurons can be measured experimentally, for the characterization of neural diseases.[40,41] Despite the enormous advances in theory and experiments, IS has not been used in the analysis of the operation of neuronal systems.

(2) A neuron undergoes a bifurcation when it is displaced between qualitatively different states by noise or external current: from rest to a spiking oscillation consisting of repetitive firing patterns. The presence of bifurcations is a key aspect to the theory of dynamical systems in neuroscience. The characterization of bifurcations in terms of impedance response has been amply studied in oscillating electrochemical systems.[42−45] According to standard methods of bifurcation theory,[46] the linearized equations for a small displacement provide important information about the nature of the trajectories in a large perturbation. Because the IS model is obtained by a linear response, the bifurcation properties of a system can be signaled by the impedance spectra on the implementation of Nyquist's stability criterion. This method has been fully developed in the field of electrochemical oscillators by Koper and others.[47−50] A chemically oscillating system or a spiking neuron is tracing a limit cycle around an unstable fixed point.[46,51] Therefore, both types of systems are controlled by similar fundamental processes that can be unified in EC representations. Chua and co-workers[52,53] applied the stability criteria of IS to show that the spiking of HH model neurons occurs in unstable regions.

(3) Once the methods described above have been outlined, the IS analysis of dynamical models of neurons can become an effective guide for the design and fabrication of artificial neurons using a variety of platforms of organic and inorganic materials. Investigating the impedance response of material devices can provide information about their dynamical response. Recently,[17] we showed the properties of IS of neuron models like HH and the adaptative integrate-and-fire model and how they relate to the halide perovskite memristor.[54]

In this paper, we describe the stability, bifurcations, and oscillations in the FHN neuron model adapted to a small signal IS method. We use the methods developed previously in the frequency domain[17] to obtain the ac impedance of a neuron model. Here we relate for the first time the impedance spectra to the spiking time dynamics of a firing neuron, by solving simultaneously the FHN neuron in the frequency and time domain. The analysis in the frequency domain provides a new angle for the study of neurons and network dynamics. We apply Koper's method of IS criteria for bifurcations of electrochemical oscillators[47−50] to dynamical neuron models. Our results show the essential structure of neuromorphic oscillatory elements such as memristors for coupled spiking networks,[55,56] in terms of the impedance properties that determine the existence of stable limit cycles.

We first describe the structure of the dynamical equations with parameters adapted to the electrical or electrochemical interpretation. Thereafter, we calculate two different measurements related to a point in the current−voltage curve. One is impedance spectroscopy by a small ac perturbation of angular frequency ω.[17] The other is voltage evolution under a large perturbation from the initial equilibrium. We show the phase plane trajectories and bifurcation behavior according to the properties of the impedance spectra.[47−50] Finally, we discuss the impedance properties that will be necessary in artificial neurons.

We formulate the FHN model equations as follows.[17,57]

$$\tau_m \frac{du}{dt} = -\frac{u^3}{3u_1^2} + u + R_I(-w + I) \tag{1}$$

$$\tau_k \frac{dw}{dt} = \frac{1}{R_w}u - bw \tag{2}$$

The physical variables are the membrane voltage u and current I and an internal recovery current w, which represents the effects of changes in ion-channel conductances that occur when the external variables are displaced to a different level. Time is reported in seconds, voltage in volts, current in amperes, and impedance in ohms. In the Supporting Information, we compare different systems of equations and parameters for the FHN model.

The independent parameters in the model of eqs 1 and 2 are voltage response time τ_m, recovery current response time τ_k, channel resistor R_I, recovery current resistor R_w, modulation constant b, and a reference voltage u_1. As w is subjected to a slow relaxation process in eq 2, it is expected that $\tau_k \gg \tau_m$ in the application of the model as an excitable neuron membrane.[58]

A series of derived parameters are useful for the physical interpretation: membrane capacitance, EC resistances, recovery current inductor, ratio of time scales, and ratio of resistances.

$$C_m = \frac{\tau_m}{R_I} \tag{3}$$

$$R_a = bR_w \tag{4}$$

$$R_b = \left(\frac{\bar{u}^2}{u_1^2} - 1\right)^{-1} R_I \tag{5}$$

$$L_a = \tau_k R_w \tag{6}$$

$$\varepsilon = \frac{\tau_m}{\tau_k} \tag{7}$$

$$r = \frac{R_I}{R_w} \tag{8}$$

In a steady state situation (indicated by an overbar), the model provides a stationary current–voltage (I–u) with the following expression

$$\bar{I} = \frac{1}{R_I}\left(\frac{\bar{u}^3}{3u_1^2} - \bar{u}\right) + \frac{1}{bR_w}\bar{u} \tag{9}$$

(a) r/b = 0.5

(b) $\dot{u} = 0$ I = 1 $\dot{w} = 0$ I = 0

(c) r/b = 1.25

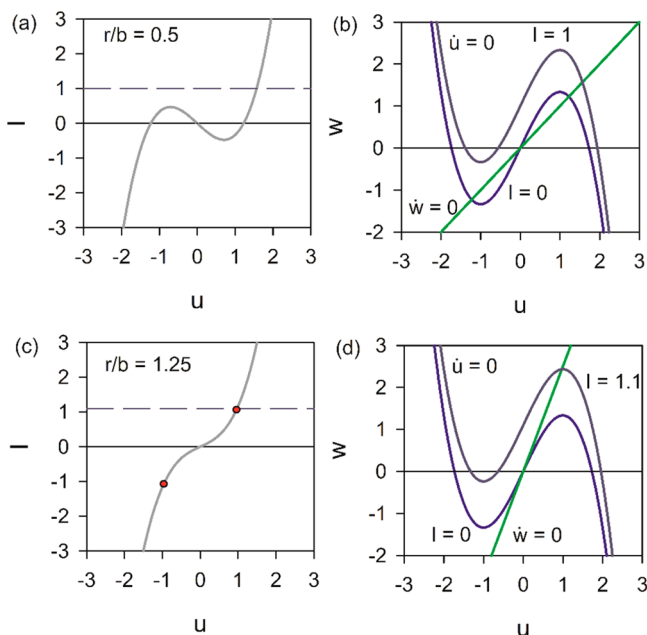(d) $\dot{u} = 0$ I = 1.1   I = 0 $\dot{w} = 0$

Figure 1. Current–voltage stationary curve and the corresponding phase plane. $R_I = 0.5$, $b = 0.8$, $\varepsilon = 0.1$, $u_1 = 1$, and two values of current as indicated (a and b) $r = 0.4$, and (c and d) $r = 1$. The red points in panel c indicate the Hopf bifurcations: $u_H = \pm 0.9591$, and $I_H = \pm 1.0678$.

Figure 1 presents the I–u curves and the phase plane of u and w for two different sets of parameters. The nullclines $\dot{w} = 0$ and $\dot{u} = 0$ have the expressions

$$w = \frac{1}{R_I}\left(-\frac{u^3}{3u_1^2} + u\right) + I \tag{10}$$

$$w = \frac{1}{bR_w}u \tag{11}$$

and the fixed points correspond to their intersections.

To obtain the response to a small perturbation, we develop linearly eqs 1 and 2, with small quantities indicated by the tilde. To calculate the ac impedance $Z = \tilde{u}/\tilde{I}$, we take the Laplace transform, $d/dt \to s$, where $s = i\omega$. Hence

$$\tau_m s\tilde{u} = \left(\frac{\bar{u}^2}{u_1^2} - 1\right)\tilde{u} - R_I\tilde{w} + R_I\tilde{I} \tag{12}$$

$$\tau_k s\tilde{w} = \frac{1}{R_w}\tilde{u} - b\tilde{w} \tag{13}$$

The result is

$$Z(s) = [R_b^{-1} + C_m s + (R_a + L_a s)^{-1}]^{-1} \tag{14}$$

The EC corresponding to eq 14 is shown in Figure 2a. It recovers the inductor introduced by Nagumo et al.[23] However, in contrast to Nagumo's circuit that contains a tunnel diode element, Figure 2a is for a small perturbation measurement and it is fully described by resistances, capacitors, and inductors that are only a function of the voltage as indicated in eqs 3–6.

Hereafter we set $u_1 = 1$ and remove the overbar; hence, eq 9 gives

$$I = \frac{1}{R_I}\left[\frac{1}{3}u^3 + \left(\frac{r}{b} - 1\right)u\right] \tag{15}$$

The dc resistance $R_{dc} = Z(\omega = 0)$ is

$$R_{dc}^{-1} = \frac{1}{R_I}\left(u^2 + \frac{r}{b} - 1\right) \tag{16}$$

The EC in Figure 2a is the same as that obtained previously for a memristive element and an integrate-and-fire neuron.[17] However, in the FHN model, there is always a negative resistance R_b in the system [in the voltage range $-1 < u < 1$ (eq 5)], corresponding to the membrane intrinsic characteristic, that provides the built-in firing mechanism. The effect of the current of recovery variable w is an added positive parallel resistance; hence, the total resistance in eq 16 may be positive or negative. A negative R_{dc} occurs when the slope of the blue curve $\dot{u} = 0$ at $u = 0$ in Figure 1 is larger than that of the green curve, which happens when $r/b < 1$ (Figure 1a). Here the current is three-valued, although at a higher current it becomes single-valued, indicating a saddle-node bifurcation.

In Figure 2b–i, we plot the impedance spectra generated by the EC in Figure 2a with different sets of parameters listed in Table 1, in the complex plane plot representation, where $Z = Z' + iZ''$. The spectra correspond to the shapes described previously.[17,59] All the spectra finish at the origin at $\omega \to \infty$ because there is no series resistance.

To analyze the stability of the fixed points, we apply a standard normal mode analysis to the linearized equations in eqs 12 and 13. The Jacobian is

$$\frac{1}{\tau_m}\begin{pmatrix} 1 - u^2 & -R_I \\ \frac{r\varepsilon}{R_I} & -b\varepsilon \end{pmatrix} \tag{17}$$

The eigenvalues λ (in units of τ_m^{-1}) are determined by the following equations

$$\lambda^2 - \tau_\lambda\lambda + \Delta = 0 \tag{18}$$

$$\lambda_{1,2} = \frac{1}{2}\left(\tau_\lambda \pm \sqrt{\tau_\lambda^2 - 4\Delta}\right) \tag{19}$$

$$\tau_\lambda = 1 - u^2 - b\varepsilon \tag{20}$$

$$\Delta = b\varepsilon\left(u^2 + \frac{r}{b} - 1\right) = b\varepsilon\frac{R_I}{R_{dc}} \tag{21}$$

$$\tau_\lambda^2 - 4\Delta = (1 - u^2 + b\varepsilon)^2 - 4r\varepsilon \tag{22}$$

These quantities are shown in Figure SI1 as a function of voltage. Note that the sign of the determinant coincides with that of the total resistance. $\Delta < 0$ corresponds to real eigenvalues $\lambda_{1,2}$ with the opposite sign. This is the region of negative R_{dc}, in which the
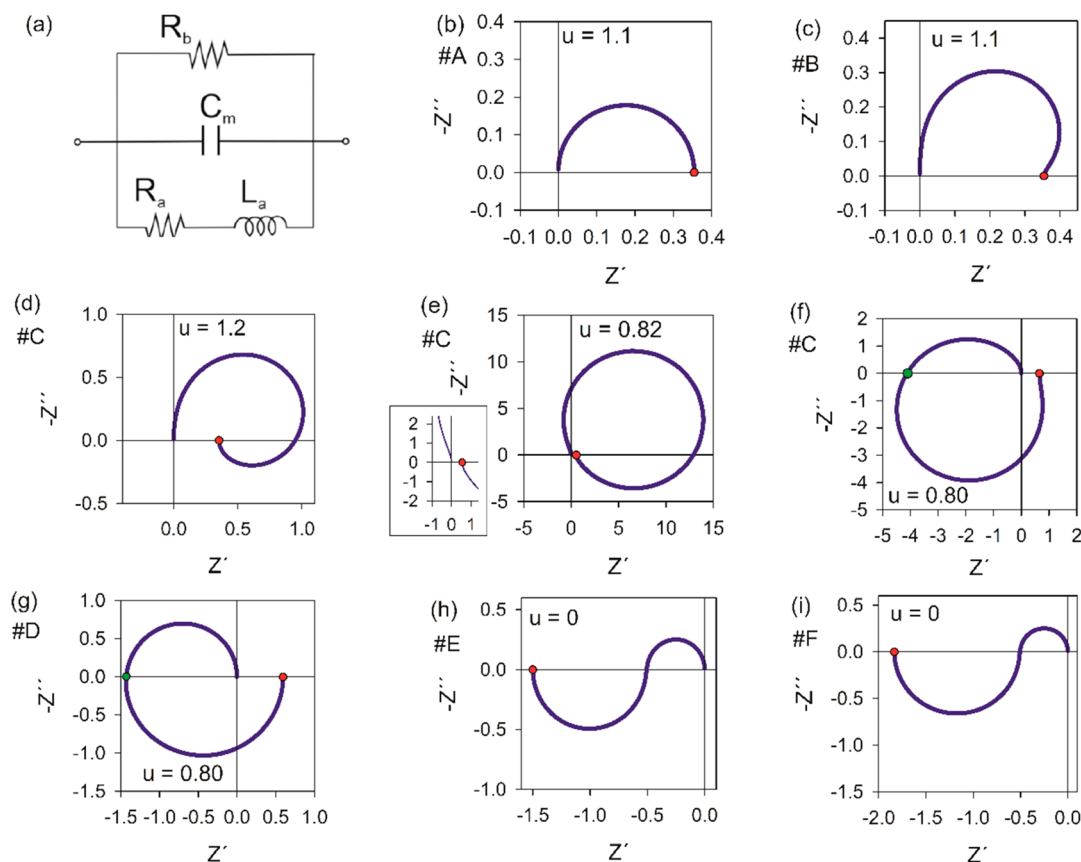
Figure 2. (a) Small ac EC for the FHN model. (b−i) Impedance spectra for different models at the indicated voltages. Panel e shows an amplification of the region close to the origin.

Table 1. Model Parameters with $R_I = 0.5\ \Omega$ and $\tau_m = 10^{-2}$ s in All Cases

model	b	r	r/b	ε	u_{Hopf}
A	1	1.2	1.2	20	
B	1	1.2	1.2	1.8	
C	1	1.2	1.2	0.316	0.82690
D	1	1.2	1.2	0.01	0.99498
E	1.2	0.8	0.66	0.01	0.99398
F	1.1	0.8	0.73	0.01	0.99448

$$\varepsilon < \frac{r}{b} \tag{23}$$

Figure 2d develops an inductive loop, while panels b and c of Figure 2 do not have such a loop. Model A in Figure 3a has $\varepsilon \gg r/b$. Here the impedance spectrum is a simple RC arc, and the trajectory (starting at the orange point) simply falls rapidly to the stable fixed point in an ordinary relaxation process. In model B of Figure 3b, the impedance spectrum bends at the real axis but does not cross it as we have $\varepsilon > r/b$. These examples do not really belong to FHN because $\varepsilon > 1$ makes w the fast variable contrary to the normal physical interpretation. We do not expect to obtain these impedance spectra in the FHN neuron, but they are shown for the sake of completeness.

In Figure 4, we change to model C with $\varepsilon < 1$ (but not very small). In Figure 4a, the current is well above the Hopf bifurcation; hence, the fixed point is a sink. Now the inductive feature in the fourth quadrant of the complex plane has been fully developed, as $\varepsilon < r/b$ is satisfied. In Figure 4b, the current is closer to the Hopf bifurcation but in the stable side, and the trajectory spirals around the fixed point and falls to it in a damped oscillation $u(t)$.

In Figure 4c, the Hopf bifurcation has been overcome. The trajectories in the phase plane change suddenly from a decay to the sink to a track around the source fixed point that never decays to it, in a stable limit cycle. The impedance pattern also changes significantly (Figure 2f,g), due to the combination of the two parallel resistive branches, a fast mode with negative resistance and a slow mode with positive resistance, the latter controlled by the series inductor.[47] Hence, the real part of the impedance becomes negative at high frequencies, in the
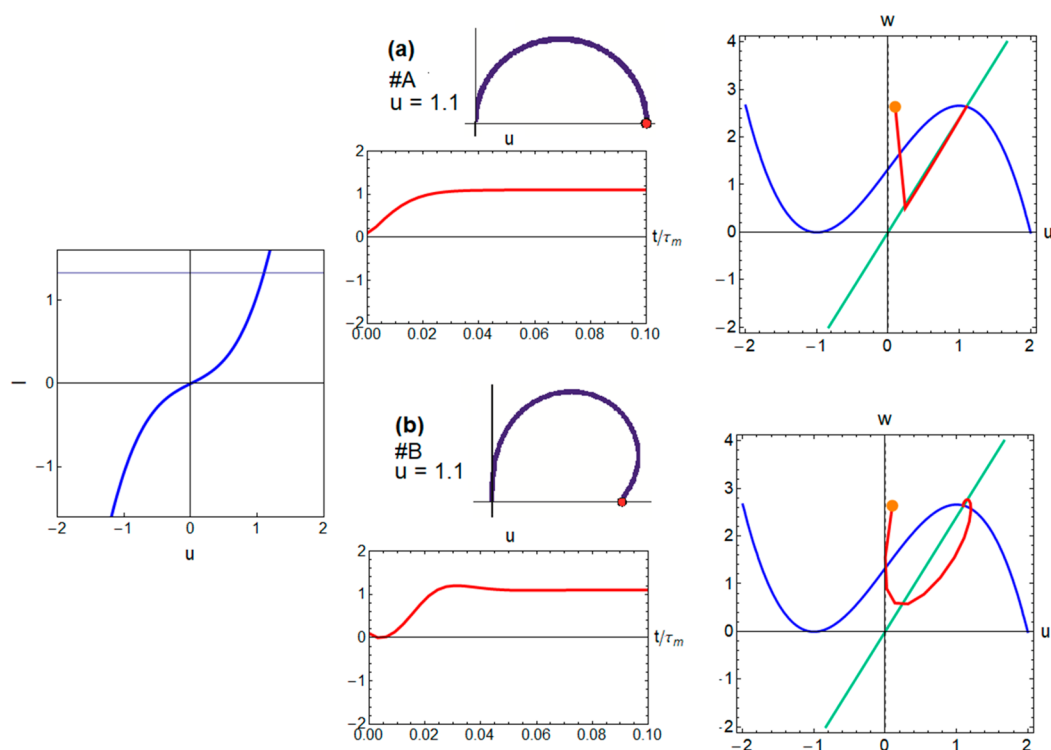
three fixed points are a saddle and two sinks. The line $r = b$ is a pitchfork bifurcation. On the contrary, $r/b > 1$ corresponds to the single-valued $I−u$ (Figure 1c) with a positive R_{dc}. Here the stability of the fixed point is determined by $\tau_\lambda < 0$. $\tau_\lambda = 0$ is the Hopf bifurcation. When $\tau_\lambda > 0$ and $\tau_\lambda^2 - 4\Delta < 0$, the fixed point becomes an unstable source with a pair of complex conjugate values $\lambda_{1,2}$. This behavior produces oscillations and spikes in $u(t)$.

We examine in the following the different situations according to the bifurcation regimes (these are classified in the Supporting Information), by solving the dynamical equations for the sets of model parameters listed in Table 1, with an initial condition $\Delta u = \pm 1$ with respect to the fixed point. A Mathematica program in the Supporting Information allows one to see the results of calculations for any chosen sets of parameters.

We start with cases of positive dc resistance $r/b > 1$. The condition for a loop in the fourth quadrant of the complex plane is $\tau_k > R_a C_m$,[17] which corresponds to

Figure 3. Voltage transients, phase plane trajectories, and impedance spectra for models with different ε values. The $I-u$ curve is the same in both cases.

intercept indicated by a green point, while it is positive at low frequencies and equal to the positive R_{dc}. This is the hidden negative impedance introduced by Koper.[59] This pattern corresponds to the limit cycle oscillations that induce neuron spiking.

In model D we change to $\varepsilon \ll 1$. In contrast to the spirals of Figure 4 obtained for $\varepsilon \approx 1$, in Figure 5 the trajectories in the phase plane become relaxation oscillations, in which the motions consist of fast horizontal portions where only u changes and the pieces of the slow mode in which w follows eq 10.

While the trajectories are discussed with respect to time, we can obtain further information about the system by analyzing the dependence of the EC elements with respect to frequency, noting that small frequencies correspond to the dynamics of longer times, and vice versa. This is shown in Figure SI2.

Finally, we take the cases in which $r/b < 1$ and $\Delta < 1$, implying that the central fixed point is an unstable saddle (Figure 6). Here $R_{dc} < 0$; hence, the impedance at low frequency starts in the negative axis of the complex plane (Figure 2h,i). The system initially sitting at the unstable $u = 0$ will jump immediately to the either of the other equilibrium points that are sinks, depending on the basin of attraction in which the initial condition sits, as shown for model E in Figure 6a. Furthermore, $I(u)$ can be measured only as a transient behavior, so that the impedance at $u = 0$ cannot be measured, unless we add a series resistances and turn the system into one in which the negative impedance is hidden as explained above. The intrinsic instability creates a rich set of dynamics. For example, a small modification from model E to model F displaces the Hopf bifurcation so that the fixed points become unstable, and the system enters limit cycle oscillations around $u = 0$ as shown in Figure 6b. Meanwhile, the impedance spectrum in Figure 6b is quite similar to the previous case.

We have classified the dynamic regimes of the FHN neuron and the associated EC and impedance spectra. The main result is

that a neuron element needs three internal components: capacitor, inductor, and negative differential resistance (NDR).

The membrane capacitance is well-known, due to the polarization by different ionic concentrations at the two sides.

The inductor element requires some explanation, as this type of inductor is unrelated to the storage of energy in a magnetic field. Recently, we showed that the inductor element is generally explained by the relaxation of the slow variable in eq 2.[17] The identification of an inductive process in the nerve membrane dates back to 1940.[60] The induction mechanism was explained by HH[18] when they proposed that the potassium conductance is proportional to a power of a variable that obeys a first-order equation, to match the very different transient curves: the delayed increase in depolarization but simple exponential decay in repolarization. Hodgkin explains very clearly in his biography[61] that "the inductance is mainly due to the delayed increase in potassium conductance which can make membrane current lag behind voltage provided the internal potential is positive to the potassium equilibrium potential." This interpretation of the inductor was supported by later measurements.[62] However, some present discussions[63] of the inductor still aim to find in neurons a magnetic coil or a piezoelectric effect. These physical properties are not needed because even minimal dynamical models generate the inductor as explained above.

Finally, the NDR is a required condition for the rhythmic oscillations, as it has been clearly recognized in the electrochemical reactions[49] and in biological neurons.[64,65]

These insights can be used for the construction of artificial neurons. On the basis of our operational understanding at the EC level, we can turn to the construction of a device and ensure that it delivers the specified operation by the reproduction of the frequency domain behavior of the target application. It is encouraging that the two first elements of the EC of a minimal neuron, namely, capacitor and inductor, have been observed in
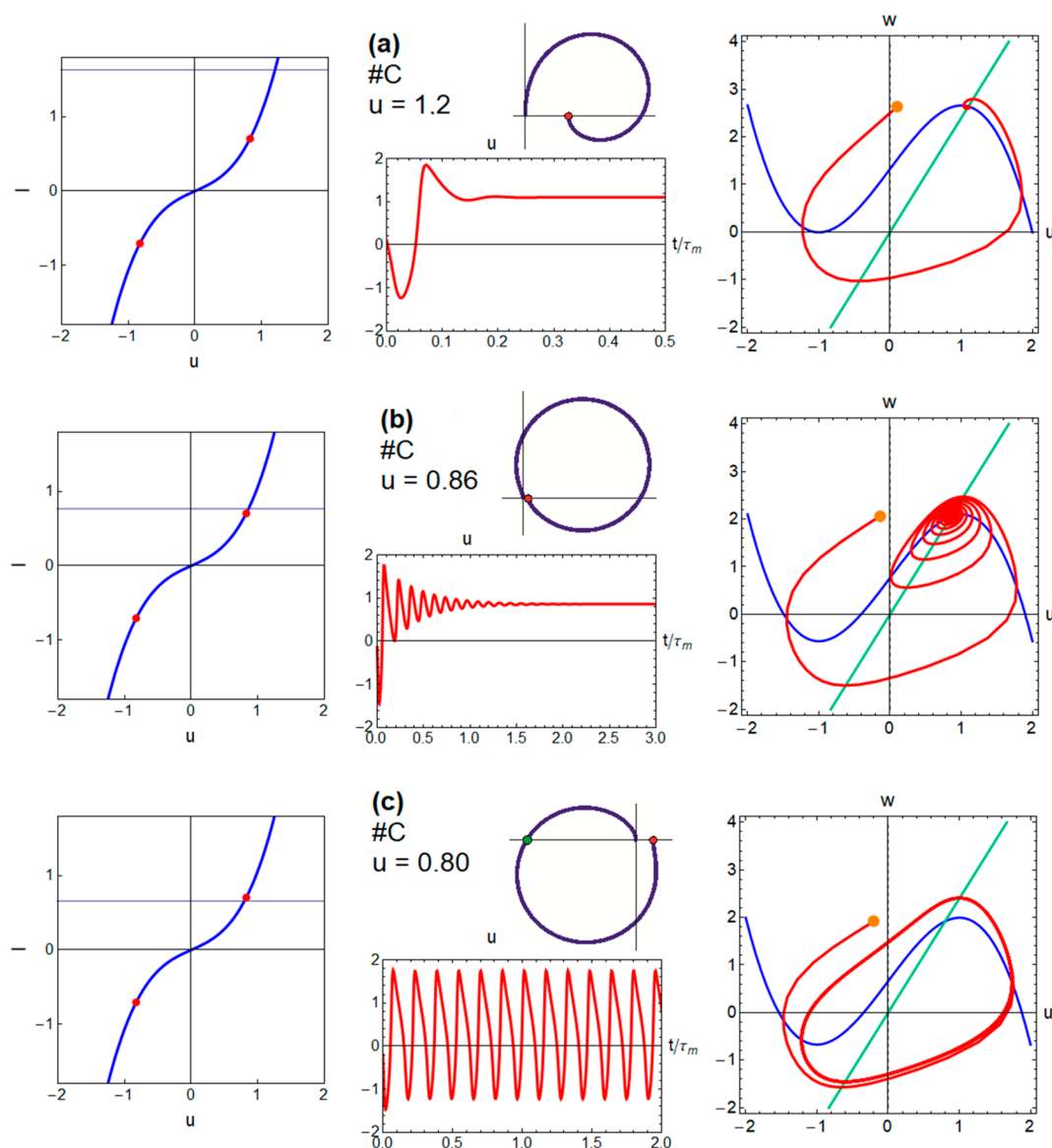
Figure 4. Voltage transients, $I-u$ curves (red points indicate the Hopf bifurcations), phase plane trajectories, and impedance spectra for model C at different voltages.
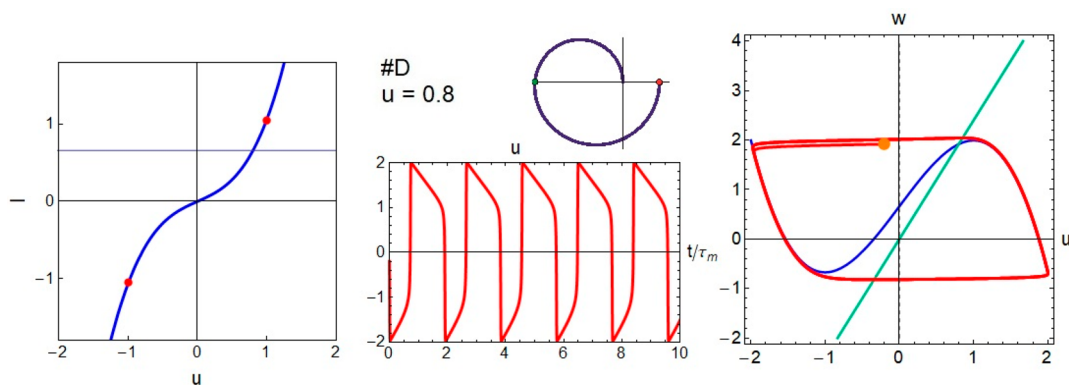

Figure 5. Voltage transient, $I-u$ curve (red points indicate the Hopf bifurcations), phase plane trajectory, and impedance spectra for model D.

halide perovskite memristors, where the inductive spectra of Figure 2d have been clearly obtained.[54] However, our results indicate the necessity of building a NDR element in the device.

In conclusion, we developed the small ac impedance that allows us to calculate the characteristic spectra of different dynamical regimes of the FitzHugh−Nagumo neuron. We could thus obtain the basic impedance response and the equivalent
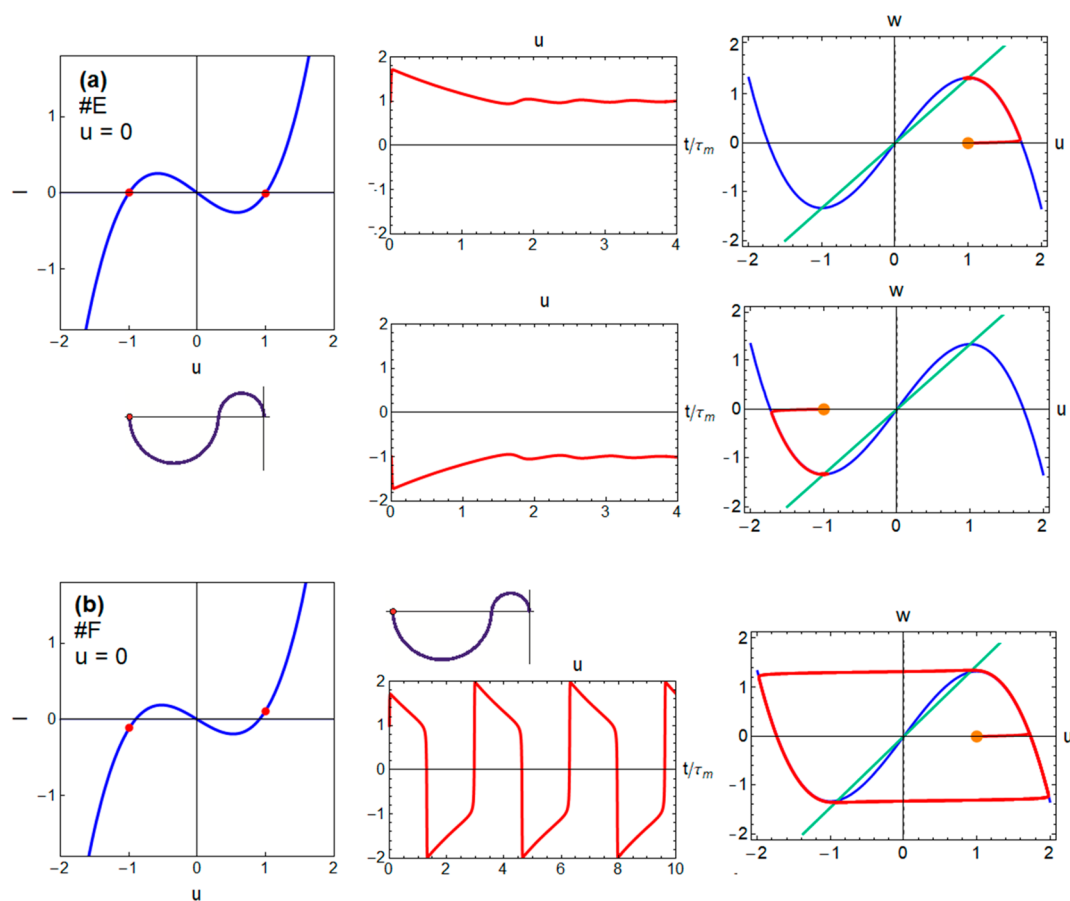
Figure 6. Voltage transients, $I-u$ curves (red points indicate the Hopf bifurcations), phase plane trajectories, and impedance spectra for (a) model E with two different initial conditions and (b) model F.

circuit of a minimal dynamical neuron model. Our results show the basic electrical structure required, consisting of some fundamental elements that give the neuron dynamics: capacitor, inductor, and at least one negative resistance. The impedance spectra immediately reveal the stability, excitability, and bifurcation properties according to the regimes of model parameters and the nature of stationary points. Here we have obtained the impedance results from a previous complete understanding of the parameters and dynamical equations. In practical operation, one can measure the impedance and reach conclusions about the physical properties based purely on the shape of experimental impedance spectra, avoiding the need for highly specific modeling. The measurement of impedance spectroscopy has the potential to become an important tool in the study of real neurons and for candidates for ionic/electronic devices to artificial spiking neurons, complementary to the usual study of transient and periodic phenomena in the time domain.

ASSOCIATED CONTENT

Supporting Information

The Supporting Information is available free of charge at https://pubs.acs.org/doi/10.1021/acs.jpclett.1c03406.

Expression of the mathematical model, bifurcation parameters, interpretation of impedance elements, Mathematica program for simulation, and graphical representation (PDF)

AUTHOR INFORMATION

Corresponding Author

Juan Bisquert — *Institute of Advanced Materials (INAM), Universitat Jaume I, 12006 Castelló, Spain;* orcid.org/0000-0003-4987-4887; Email: bisquert@uji.es

Complete contact information is available at:
https://pubs.acs.org/10.1021/acs.jpclett.1c03406

Notes

The author declares no competing financial interest.

REFERENCES

(1) Stiefel, K. M.; Ermentrout, G. B. Neurons as oscillators. *J. Neurophysiol.* **2016**, *116*, 2950−2960.

(2) Posch, C.; Serrano-Gotarredona, T.; Linares-Barranco, B.; Delbruck, T. Retinomorphic event-based vision sensors: Bioinspired cameras with spiking output. *Proc. IEEE* **2014**, *102*, 1470−1484.

(3) Mead, C. Neuromorphic electronic systems. *Proc. IEEE* **1990**, *78*, 1629−1636.

(4) Merolla, P. A.; Arthur, J. V.; Alvarez-Icaza, R.; Cassidy, A. S.; Sawada, J.; Akopyan, F.; Jackson, B. L.; Imam, N.; Guo, C.; Nakamura, Y.; et al. A million spiking-neuron integrated circuit with a scalable communication network and interface. *Science* **2014**, *345*, 668−673.

(5) Davies, M.; Srinivasa, N.; Lin, T. H.; Chinya, G.; Cao, Y.; Choday, S. H.; Dimou, G.; Joshi, P.; Imam, N.; Jain, S.; et al. Loihi: A neuromorphic manycore processor with on-chip learning. *IEEE Micro* **2018**, *38*, 82−99.

(6) Furber, S. B.; Galluppi, F.; Temple, S.; Plana, L. A. The SpiNNaker project. *Proc. IEEE* **2014**, *102*, 652−665.

(7) Maass, W. Networks of spiking neurons: The third generation of neural network models. *Neural Networks* **1997**, *10*, 1659−1671.

(8) Linares-Barranco, B. Memristors fire away. *Nat. Electron.* **2018**, *1*, 100−101.

(9) Indiveri, G.; Linares-Barranco, B.; Legenstein, R.; Deligeorgis, G.; Prodromakis, T. Integration of nanoscale memristor synapses in neuromorphic computing architectures. *Nanotechnology* **2013**, *24*, 384010.

(10) Johnson, B. A.; Brahim, K.; Balanov, A. G.; Savel'ev, S.; Borisov, P. Transition from noise-induced to self-sustained current spiking generated by a NbO$_x$ thin film threshold switch. *Appl. Phys. Lett.* **2021**, *118*, 023502.

(11) Gao, L.; Chen, P.-Y.; Yu, S. NbO$_x$ based oscillation neuron for neuromorphic computing. *Appl. Phys. Lett.* **2017**, *111*, 103503.

(12) Lasia, A. *Electrochemical Impedance Spectroscopy and its Applications*; Springer, 2014.

(13) Grimnes, S.; Martinsen, O. G. *Bioimpedance and Bioelectricity Basics*, 3rd ed.; Academic Press, 2015.

(14) Stupin, D. D.; Kuzina, E. A.; Abelit, A. A.; Emelyanov, A. K.; Nikolaev, D. M.; Ryazantsev, M. N.; Koniakhin, S. V.; Dubina, M. V. Bioimpedance Spectroscopy: Basics and Applications. *ACS Biomater. Sci. Eng.* **2021**, *7*, 1962−1986.

(15) Xu, Y.; Xie, X.; Duan, Y.; Wang, L.; Cheng, Z.; Cheng, J. A review of impedance measurements of whole cells. *Biosens. Bioelectron.* **2016**, *77*, 824−836.

(16) Spencer, D. C.; Paton, T. F.; Mulroney, K. T.; Inglis, T. J. J.; Sutton, J. M.; Morgan, H. A fast impedance-based antimicrobial susceptibility test. *Nat. Commun.* **2020**, *11*, 5328.

(17) Bou, A.; Bisquert, J. Impedance spectroscopy dynamics of biological neural elements: from memristors to neurons and synapses. *J. Phys. Chem. B* **2021**, *125*, 9934−9949.

(18) Hodgkin, A. L.; Huxley, A. F. A quantitative description of membrane current and its application to conduction and excitation in nerve. *J. Physiol.* **1952**, *117*, 500−544.

(19) Pallotta, B. S.; Wagoner, P. K. Voltage-dependent potassium channels since Hodgkin and Huxley. *Physiol. Rev.* **1992**, *72*, S49−S67.

(20) Hermann, L. Beitrage zur physiologie und physik des nerven. *Pfluegers Arch.* **1905**, *109*, 95−144.

(21) Philippson, M. Les lois de la resistance electrique des tissus vivants. *Bull. Acad. R. Belg. Clin. Sci.* **1921**, *7*, 387−403.

(22) Lapicque, L. Recherches quantitatives sur l'excitation electrique des nerfs traite'e comme une polarization. *J. Physiol. Pathol. Gen.* **1907**, *9*, 620−635.

(23) Yamakou, M. E.; Tran, T. D.; Duc, L. H.; Jost, J. The stochastic Fitzhugh−Nagumo neuron model in the excitable regime embeds a leaky integrate-and-fire model. *J. Math. Biol.* **2019**, *79*, 509−532.

(24) Morris, C.; Lecar, H. Voltage oscillations in the barnacle giant muscle fiber. *Biophys. J.* **1981**, *35*, 193−213.

(25) Nagumo, J.; Arimoto, S.; Yoshizawa, S. An active pulse transmission line simulating nerve axon. *Proc. IRE* **1962**, *50*, 2061−2070.

(26) Izhikevich, E. M. Simple model of spiking neurons. *IEEE Trans. Neural Networks* **2003**, *14*, 1569−1572.

(27) Izhikevich, E. M. *Dynamical Systems in Neuroscience*; MIT Press, 2007.

(28) FitzHugh, R. Impulses and physiological states in theoretical models of nerve membrane. *Biophys. J.* **1961**, *1*, 445−466.

(29) Rocşoreanu, C.; Georgescu, A.; Giurgiţeanu, N. *The FitzHugh-Nagumo Model: Bifurcation and Dynamics*; Kluwer Academic Publishers, 2000.

(30) Kostova, T.; Ravindran, R.; Schonbek, M. Fitzhugh−Nagumo revisited: types of bifurcations, periodical forcing and stability regions by a Lyapunov functional. *Int. J. Bifurcation Chaos Appl. Sci. Eng.* **2004**, *14*, 913−925.

(31) Armbruster, D. The (almost) complete dynamics of the Fitzhugh-Nagumo equations. *Nonlinear Dynam.* **1997**, *2*, 89−102.

(32) Burić, N.; Todorović, D. Dynamics of FitzHugh-Nagumo excitable systems with delayed coupling. *Phys. Rev. E: Stat. Phys., Plasmas, Fluids, Relat. Interdiscip. Top.* **2003**, *67*, 066222.

(33) Mao, X.; Sun, J.; Li, S. Dynamics of delay-coupled FitzHugh-Nagumo neural rings. *Chaos* **2018**, *28*, 013104.

(34) Wang, Q.; Lu, Q.; Chen, G.; Feng, Z.; Duan, L. Bifurcation and synchronization of synaptically coupled FHN models with time delay. *Chaos, Solitons Fractals* **2009**, *39*, 918−925.

(35) Fan, D.; Hong, L. Hopf bifurcation analysis in a synaptically coupled FHN neuron model with delays. *Commun. Nonlinear Sci. Numer. Sim.* **2010**, *15*, 1873−1886.

(36) Zhen, B.; Xu, J. Simple zero singularity analysis in a coupled FitzHugh−Nagumo neural system with delay. *Neurocomputing* **2010**, *73*, 874−882.

(37) Song, Y.; Xu, J. Inphase and antiphase synchronization in a delay-coupled system with applications to a delay-coupled FitzHugh−Nagumo system. *IEEE Transactions on Neural Networks and Learning Systems* **2012**, *23*, 1659−1670.

(38) Farajzadeh Tehrani, N.; Razvan, M. Bifurcation structure of two coupled FHN neurons with delay. *Math. Biosci.* **2015**, *270*, 41−56.

(39) Ibrahim, M. M.; Kamran, M. A.; Mannan, M. M. N.; Jung, I. H.; Kim, S. Lag synchronization of coupled time-delayed FitzHugh−Nagumo neural networks via feedback control. *Sci. Rep.* **2021**, *11*, 3884.

(40) Thakore, V.; Molnar, P.; Hickman, J. J. An optimization-based study of equivalent circuit models for representing recordings at the neuron−electrode interface. *IEEE Trans. Biomed. Eng.* **2012**, *59*, 2338−2347.

(41) Massobrio, G.; Martinoia, S.; Massobrio, P. Equivalent circuit of the neuro-electronic junction for signal recordings from planar and engulfed micro-nano-electrodes. *IEEE Trans. Biomed. Circuits Syst.* **2018**, *12*, 3−12.

(42) Sadkowski, A.; Dolata, M.; Diard, J. P. Kramers-Kronig transforms as validation of electrochemical immittance data near discontinuity. *J. Electrochem. Soc.* **2004**, *151*, E20.

(43) Sadkowski, A. Small signal local analysis od electrocataytical reaction. Pole-zero approach. *J. Electroanal. Chem.* **1999**, *465*, 119−128.

(44) Strasser, P.; Eiswirth, M.; Ertl, G. Oscillatory instabilities during formic acid oxidation on Pt(100), Pt(110) and Pt(111) under potentiostatic control. II. Model calculations. *J. Chem. Phys.* **1997**, *107*, 991−1003.

(45) Strasser, P.; Eiswirth, M.; Koper, M. T. M. Mechanistic classification of electrochemical oscillators-an operational experimental strategy. *J. Electroanal. Chem.* **1999**, *478*, 50.

(46) Strogatz, S. H. *Nonlinear Dynamics and Chaos*, 2nd ed.; CRC Press, 2019.

(47) Koper, M. T. M. Oscillations and complex dynamical bifurcations in electrochemical systems. *Adv. Chem. Phys.* **2007**, *92*, 161.

(48) Koper, M. T. M. Non-linear phenomena in electrochemical systems. *J. Chem. Soc., Faraday Trans.* **1998**, *94*, 1369−1378.

(49) Krischer, K. Nonlinear Dynamics in Electrochemical Systems. *Advances in Electrochemical Science and Engineering* **2002**, 89−208.

(50) Orlic, M. *Self-Organization in Electrochemical Systems I*; Springer, 2012.

(51) Scott, S. K. *Chemical Chaos*; Clarendon Press, 1991.

(52) Chua, L.; Sbitnev, V.; Kim, H. Hodgkin−Huxley axon is made of memristors. *Int. J. Bifurcation Chaos Appl. Sci. Eng.* **2012**, *22*, 1230011.

(53) Chua, L.; Sbitnev, V.; Kim, H. Neurons are poised near the edge of chaos. *Int. J. Bifurcation Chaos Appl. Sci. Eng.* **2012**, *22*, 1250098.

(54) Gonzales, C.; Guerrero, A.; Bisquert, J. Spectral properties of the dynamic state transition in metal halide perovskite-based memristor exhibiting negative capacitance. *Appl. Phys. Lett.* **2021**, *118*, 073501.

(55) Ushakov, Y.; Akther, A.; Borisov, P.; Pattnaik, D.; Savel'ev, S.; Balanov, A. G. Deterministic mechanisms of spiking in diffusive memristors. *Chaos, Solitons Fractals* **2021**, *149*, 110997.

(56) Zhang, X.; Zhuo, Y.; Luo, Q.; Wu, Z.; Midya, R.; Wang, Z.; Song, W.; Wang, R.; Upadhyay, N. K.; Fang, Y.; et al. An artificial spiking afferent nerve based on Mott memristors for neurorobotics. *Nat. Commun.* **2020**, *11*, 51.

(57) Gerstner, W.; Kistler, W. M.; Naud, R.; Paninski, L. *Neuronal Dynamics. From Single Neurons to Networks and Models of Cognition*; Cambridge University Press, 2014.

(58) Kuehn, C. *Multiple Time Scale Dynamics*; Springer, 2015.

(59) Koper, M. T. M.; Sluyters, J. H. Instabilities and oscillations in simple models of electrocatalytic surface reactions. *J. Electroanal. Chem.* **1994**, *371*, 149.

(60) Cole, K. S. Rectification and inductance in the squid giant axon. *J. Gen. Physiol.* **1941**, *25*, 29−51.
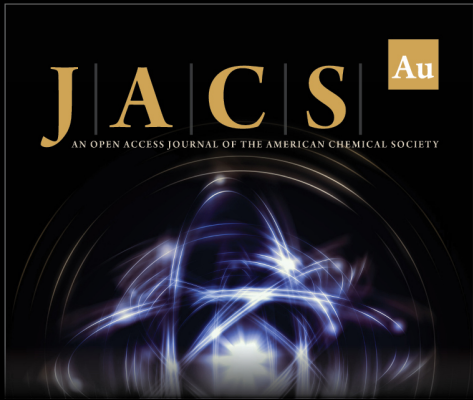
(61) Hodgkin, A. *Chance and Design: Reminiscences of Science in Peace and War Illustrated Edition*; Cambridge University Press, 1992.

(62) Homblé, F.; Jenard, A. Pseudo-inductive behaviour of the membrane potential of chara corallina under galvanostatic conditions: A time-variant conductance property of potassium channels. *J. Exp. Bot.* **1984**, *35*, 1309−1322.

(63) Wang, H.; Wang, J.; Cai, G.; Liu, Y.; Qu, Y.; Wu, T. A Physical perspective to the inductive function of myelin—a missing piece of neuroscience. *Front. Neural Circuits* **2021**, *14*, 562005.

(64) Wilson, W. A.; Wachtel, H. Negative resistance characteristic essential for the maintenance of slow oscillations in bursting neurons. *Science* **1974**, *186*, 932−934.

(65) Barra, P. F. A. The action potentials and currents on the I-V plane in the molluscan neuron. *Comp. Biochem. Physiol. A* **1997**, *116*, 313−321.